Suppression of force fluctuations in flow past an aerofoil

A. Conlin and X. Mao

School of Engineering and Computing Sciences, Durham University, Durham, DH1 3LE, UK

Force fluctuations on a solid body are associated with unsteadiness in the wake, e.g. vortex shedding. Therefore the control of force fluctuations can be realised by suppressing the flow unsteadiness. A NACA0024 aerofoil closed with a round trailing edge is chosen to represent the solid body throughout this investigation, with the Reynolds number fixed at $Re = 1000$ and angle of attack $\alpha \leq 15^o$, at which the uncontrolled flow is two-dimensional. A linear optimal control is calculated by analysing the distribution of sensitivity of unsteadiness to control around the entire surface of the body. The nonlinear effects of the calculated control, which can be actuated through surface-normal suction and blowing across the surface of the aerofoil, are tested through two-dimensional direct numerical simulations. It is observed that a surface-normal velocity control with a maximum magnitude less than 8% of the free stream velocity completely suppresses unsteadiness at $\alpha = 10°$ with an overall drag reduction of 14% and a 138% increase of lift.

Keywords: Sensitivity, vortex shedding, drag reduction

1.   Introduction

Wind turbine blades along with other structures such as bridges and multi-storey buildings can be subject to resonant wind conditions, leading to unexpected structure responses and in some cases, permanent deformations. When flow passes a turbine blade at large angles of attack, vortices shed periodically off the body, which alters the pressure distribution and causes the blade to experience a time-varying force at the same frequency as the vortex shedding (King 1977). Although the persistent periodic nature and excellent mixing qualities of vortex streets can be useful for certain applications (Ahlborna, Setob and Noackc 2002), the adverse effects of vortex shedding are amplified when the frequency of shedding is close to the frequency of the structural oscillation, otherwise known as the "lock-in" effect; a phenomena that could lead to catastrophic structural behaviors.

  Visualization techniques have been used extensively to investigate the flow patterns and effects associated with vortex shedding since the days of Leonardo Da Vinci (Bearman and Graham 1980; Perry, Chong and Lim 1982). The research into the control of vortex shedding has largely been split up into two categories: passive control and active control. Passive controls such as splitter plates (Bearman 1965; Kwon and Choi 1995), shrouds (Zdravkovich 1981), riblets (Chamorro, Arndt, and Sotiropoulos 2013) and secondary control cylinders (Mittal and Raghuvanshi 2001) rely on geometric adaptations to modify the flow, e.g. the boundary layer, separation and vortex shedding. Active controls involve injecting energy into the boundary layer via mechanisms such as moving surfaces (Skote 2013; Ricco and Hahn 2013) or suction and blowing (Raju, Mittal and Cattafesta 2008). For the two-dimensional flow considered in this work, two types of control can be defined

---

*Corresponding author. Email:xuerui.mao@durham.ac.uk
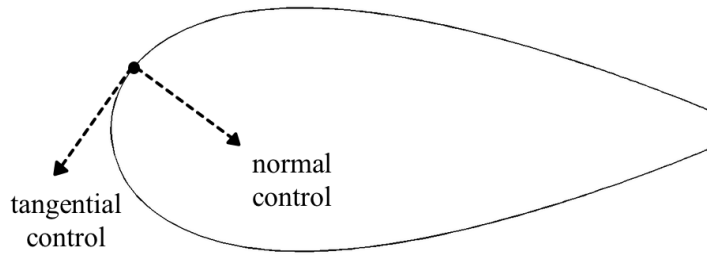
Figure 1.: Sketch showing the direction of two surface velocity controls.

depending on the direction of the control velocity with respect to the body surface: normal control and tangential control, as illustrated in figure 1.

Tangential control has been known to be effective in suppressing vortex shedding and drag reductions. The technique involves injecting momentum into the boundary layer through the application of moving surfaces. This concept was discussed by Modi and Yokomizo (1994) in a study that focused on moving surface boundary layer control (MSBC) which reduced drag by 75% on a flat plate. For aerofoil flow, this technique can be implemented by placing rotating cylinders at the leading edge of an aerofoil (Ongoren and Rockwell 1988; Tokumaru and Dimotakis 1991). It has been shown that rolling cylinders generate effective control irrespective of the wind direction, speed or the structural frequencies involved (Kubo et al. 1992).

For the normal control, it has been shown that a steady blowing control around the trailing edge of a circular cylinder can stabilise the wake and is energetically more efficient than suction (Delaunay and Kaiktsis 2001). Other studies have shown that periodic normal control can suppress wake disturbances with significantly less energy injection than steady normal control (Raju, Mittal and Cattafesta 2008; Seifert, Darabi and Wygnanski 1996). This frequency dependence of the control effects is studied in the current work in the linear regime.

In the rest of this work, the methodology associated with calculating the control is discussed in section 2, followed by a description of the discretisation in section 3. Then the uncontrolled flow, distributions of the optimal control and the control effects are discussed in section 4.

2.   Methodology

2.1.   *Governing equations*

The controlled flow can be regarded as the sum of the uncontrolled flow $(\boldsymbol{U}, P)$ and control induced flow $(\boldsymbol{u}, p)$:

$$(\hat{\boldsymbol{u}}, \hat{p}) = (\boldsymbol{U}, P) + (\boldsymbol{u}, p)$$

where $\hat{\boldsymbol{u}}, \boldsymbol{U}$ and $\boldsymbol{u}$ are total, uncontrolled and control induced velocities respectively and $\hat{p}, P$ and p are the total, uncontrolled and control induced pressures respectively. The control induced velocity and pressure with small enough magnitude are governed by the linearised Navier-Stokes (NS) equation:

$$\partial_t \boldsymbol{u} + \boldsymbol{U} \cdot \boldsymbol{\nabla} \boldsymbol{u} + \boldsymbol{u} \cdot \boldsymbol{\nabla} \boldsymbol{U} + \boldsymbol{\nabla} p - Re^{-1} \nabla^2 \boldsymbol{u} = 0 \qquad \text{with} \qquad \nabla \cdot \boldsymbol{u} = 0.$$

The control induced velocity is assumed to be zero at the beginning of the simulation and therefore $\boldsymbol{u}$ is initialized to be zero. For the boundary conditions, zero Dirichlet (velocity) and computed Neumann (pressure) conditions are adopted on the inflow and far field boundaries whereas zero Neumann (velocity) and zero Dirichlet (pressure) conditions are implemented on the outflow boundary.
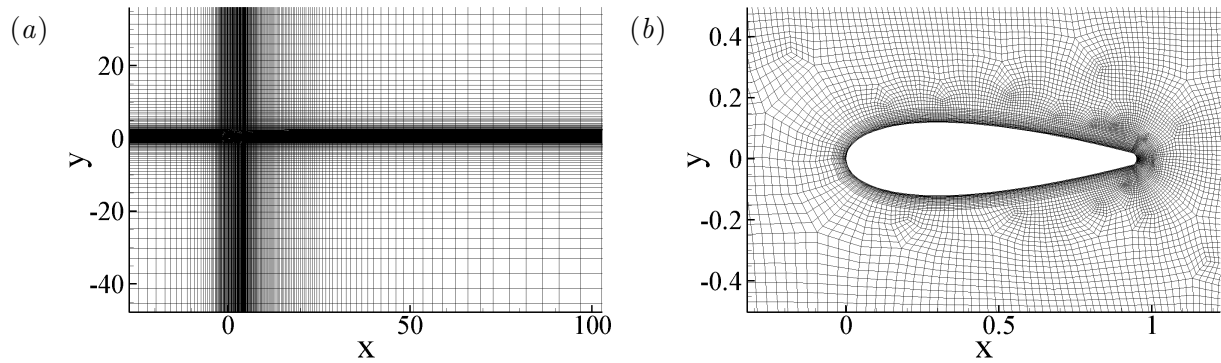
Figure 2.: Computational mesh around the modified NACA0024 aerofoil for (a) the entire domain (b) the sub-domain around the aerofoil.

Dirichlet (velocity) and Neumann (pressure) conditions are used on the controlled boundary which refers to the surface of the body and is denoted as $\boldsymbol{C}$ in the following.

2.2. Control modeling

For the two-dimensional geometry considered in this work, the control can be in form of surface velocity normal or tangential to the aerofoil. The normal control can be physically implemented by steady jets or synthetic jets (driven by oscillating membranes in a cavity) while the tangential control can be generated by rolling cylinders or electromagnetic devices. Since a distributed normal control with different magnitude along the aerofoil is much easier to generate than a tangential control, only the normal control is considered here, even though the tangential control can be calculated in a similar manner. For the surface normal control, a decomposition of the temporal and spatial dependence is necessary to reduce the dimension of the body-surface velocity after spatial-temporal discretisation

$$\boldsymbol{u}\left(\boldsymbol{C},t\right) = G\left(t\right)u_n\left(\boldsymbol{C}\right)\boldsymbol{n} \tag{1}$$

where $u_n(\boldsymbol{C})$ is the spatial dependence of the surface velocity, $\boldsymbol{n}$ denotes the unit outward normal vector and $G(t)$ is a temporal dependence function defined as

$$G(t) = \text{Real}\left((1 - \mathrm{e}^{-\sigma t^2})\mathrm{e}^{\mathrm{i}\omega t}\right)$$

where σ acts as a relaxation factor and $\sigma = 100$ is adopted throughout this work; ω is the frequency of the surface velocity control. This temporal function results in a zero control at $t = 0$, which is consistent with the zero initial condition for the control induced velocity $\boldsymbol{u}$.

The optimal distribution of $u_n(\boldsymbol{C})$ is referred to as the optimal control (with frequency ω) in this study. The magnitude of this optimal control is calculated as the square root of the square integration of the control along the surface of the body and is denoted as the control-boundary norm throughout this work,

$$||u_n||_c = \left(\int u_n^2 \, d\boldsymbol{C}\right)^{1/2}.$$

3

2.3. *Sensitivity of unsteadiness to surface control*

The main idea of this work involves developing a control to suppress unsteadiness in the flow and therefore eliminate the force fluctuations. Unsteadiness can be calculated in terms of the fluctuation energy which is the difference between the total and average kinetic energy in the system. This is defined on the temporal interval $[0,\tau]$ and spatial domain Ω and can be written as

$$A\left(\boldsymbol{u}\right) = \frac{1}{\tau}\int_0^\tau \int_\Omega \hat{\boldsymbol{u}} \cdot \hat{\boldsymbol{u}} \mathrm{d}V \mathrm{d}t - \int_\Omega \hat{\boldsymbol{u}_a} \cdot \hat{\boldsymbol{u}_a} \mathrm{d}V.$$

The first term on the right side is the total kinetic energy and the second is the energy of the time-averaged flow, whose velocity is denoted as $\hat{\boldsymbol{u}_a}$. This fluctuation energy A is the objective function that will be minimised under the optimal control. It is noticed that the unsteadiness far away from the body has limited influence to the fluctuation of the force acting on the body and therefore can be filtered. The gradient of the unsteadiness A is evaluated with respect to the control,

$$\boldsymbol{\nabla}_{\boldsymbol{u}_n} A = \tau^{-1}\boldsymbol{n} \cdot \int_0^\tau \left(p^*\boldsymbol{n} - Re^{-1}\boldsymbol{\nabla}_{\boldsymbol{n}}\boldsymbol{u^*}\right) G(-t)\mathrm{d}t,$$

where $\boldsymbol{u^*}$ and p^* are the adjoint velocity and pressure variables respectively obtained by integrating the adjoint equation

$$\partial_t\boldsymbol{u^*} + \boldsymbol{U}\cdot\boldsymbol{\nabla}\boldsymbol{u^*} - \boldsymbol{\nabla}\boldsymbol{U}\cdot\boldsymbol{u^*} - \boldsymbol{\nabla}p^* + Re^{-1}\nabla^2\boldsymbol{u^*} + 2\left(\boldsymbol{U} - \boldsymbol{U_a}\right) = 0 \qquad \text{and} \qquad \boldsymbol{\nabla}\cdot\boldsymbol{u^*} = 0, \quad (2)$$

with $\boldsymbol{U_a}$ denoting the average of the uncontrolled flow. It is noticed that this gradient $\boldsymbol{\nabla}_{\boldsymbol{u}_n} A$ represents the sensitivity of the unsteadiness with respect to the boundary control. The algorithm to calculate the sensitivity via integrating the adjoint equation is documented in Mao, Blackburn and Sherwin (2015) and will not be elaborated here.

3.   Discretisation

In this study, a NACA0024 aerofoil is adopted as an example of a solid body. This relatively thick aerofoil is closed with a round trailing edge so as to reduce the maximum curvature of the geometry and facilitate the numerical calculations of the distribution of the optimal control, which requires a smooth controlled boundary. This modification of the trailing edge reduces the chord length to 0.95. As shown in figure 2, the leading edge is positioned at $(x, y) = (0, 0)$ and the entire surface of the aerofoil is considered to be the controlled boundary $\boldsymbol{C}$. Throughout this work, the Reynolds number is fixed at $Re = 1000$, at which the uncontrolled flow is two-dimensional over the range of angles of attack considered, i.e. $0° \leq \alpha \leq 15°$, even when the computational domain is extended in the spanwise direction to be three-dimensional. It has been observed that at $Re = 2000$ and $\alpha = 10^o$ (the dominant angle of attack considered here) the uncontrolled flow becomes unstable to three-dimensional disturbance and develops into spanwise varying flow. The sensitivity calculation based on a three-dimensional uncontrolled flow requires much larger memory to save the uncontrolled flow than the two-dimensional cases. Therefore the three-dimensional flow at higher Reynolds number is not investigated in this work. However, as most of the stability and DNS work, we assume that the result of the low Reynolds number flow could shed light on the understanding of large Reynolds number flow.

A well-tested code, i.e. SEMTEX, based on a spectral h/p element method, is used to solve the governing equations, e.g. the NS and the adjoint equations. Figure $2(a)$ shows the entire domain containing 5815 spectral elements while figure $2(b)$ gives a close up view of the spectral element decomposition around the aerofoil. In each element, a fifth-order polynomial expansion, at which the magnitude of the sensitivity converges to three significant figures, is adopted.
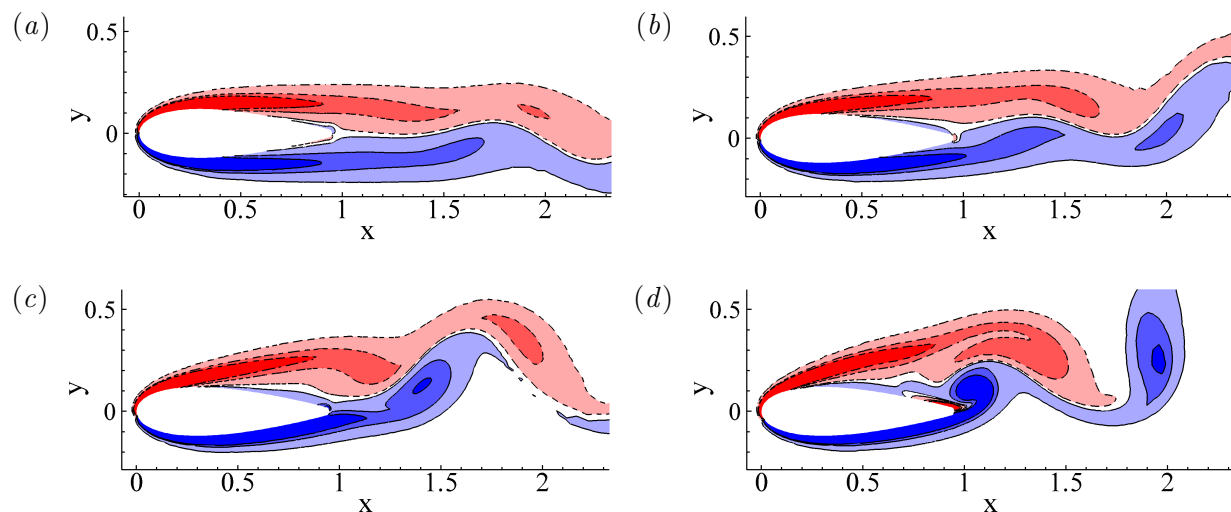
Figure 3.: Contours of uncontrolled spanwise vorticity at angle of attack (a) $\alpha = 0°$, (b) $\alpha = 5°$, (c) $\alpha = 10°$ and (d) $\alpha = 15°$. Solid and dashed lines represent positive and negative vorticity respectively and the contour levels used are [-10 -6 -1 1 6 10], which will be adopted for all further vorticity plots. The Reynolds number is fixed at $Re = 1000$ in this and all following figures.

4.   Results and Discussions

4.1.   *Uncontrolled flow*

The uncontrolled flow around the aerofoil can be obtained using two-dimensional direct numerical simulations (2D DNS) until a periodic state is reached. This uncontrolled velocity is saved and used to solve the adjoint variables via an integration of the adjoint equation (2). Figure 3 shows the vorticity contours of the uncontrolled (base) flow at $\alpha = 0°$, $\alpha = 5°$, $\alpha = 10°$, and $\alpha = 15°$. It can be seen from figure 3(a) that at $\alpha = 0°$, weak vortex shedding resides downstream of the body and therefore has negligible effects on the forces acting on the surface. As the angle of attack increases, the amplitude of the shedding increases and appears closer to the trailing edge of the body. By $\alpha = 10°$ as shown in figure 3(c), the flow separation induces strong shedding propagating from the upper surface of the aerofoil. It is clear from the analysis of the base flow that at $\alpha = 0°$ and $\alpha = 5°$ the velocity fluctuations are small and consequently the force fluctuations are also small, as will be verified later in figure 9. Therefore the $\alpha = 10°$ case is adopted as the defaulted case to study the force fluctuation associated with vortex shedding in the following if not otherwise stated.

4.2.   *Sensitivity of unsteadiness to control*

From the magnitude of the sensitivity of unsteadiness with respect to surface-normal control, or the control-boundary norm of the sensitivity as shown in figure 4, it is seen that the sensitivity at $\alpha = 10^o$ reaches local maxima at three frequencies, i.e. $\omega = 0$, $\omega = 4.4$, which is the vortex shedding frequency of the uncontrolled flow, and $\omega = 8.8$. The linear optimal control can be obtained by scaling (and reversing) the sensitivity (Mao and Pearson 2015). Therefore these frequencies correspond to steady control, periodic control at the dominant frequency of the uncontrolled flow and periodic control at a higher harmonic of the dominant frequency respectively. For the steady case with $\omega = 0$ the corresponding control is robust as it is effective irrespective of when the control is imposed on the shedding cycle. On the other hand, the periodic controls are sensitive to the start time and could increase or decrease the unsteadiness depending on the time at which the control is imposed, since these controls reverse every half of the period. Therefore $\omega = 0$ will be used as the
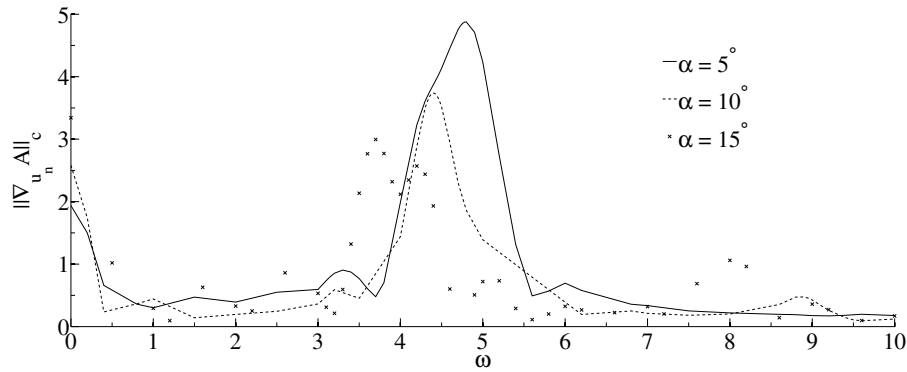
Figure 4.: Control-boundary norm of the sensitivity of unsteadiness with respect to surface-normal control.
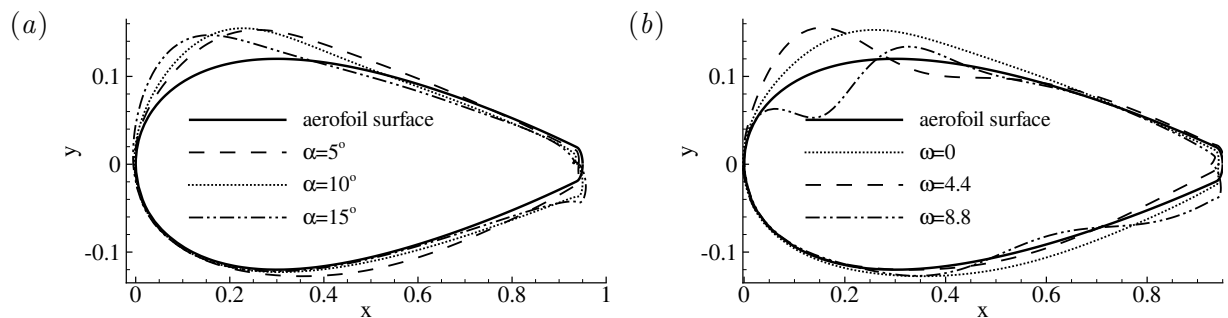
Figure 5.: Distributions of the sensitivity with respect to normal control for (a) $\omega = 0$ and various angles of attack, (b) $\alpha = 10^o$ and various control frequencies.

defaulted frequency in the following investigations.

Figure 5(a) and 5(b) provide a visual representation of the distribution of the sensitivity or the linear optimal control. This visualization is obtained by adding to the body surface the normalized sensitivity with a control-boundary norm of 0.02 so that the sensitivity curves can be expressed as $\boldsymbol{C} + 0.02\boldsymbol{\nabla}_{u_n}A/||\boldsymbol{\nabla}_{u_n}A||_c$. Deviation from the aerofoil surface $\boldsymbol{C}$ corresponds to the magnitude and distribution of the sensitivity; lines outside the surface represent a negative sensitivity which is associated with blowing, whereas lines inside the surface represent positive sensitivity corresponding to suction. Figure 5(a) shows the variation of sensitivities with respect to the angle of attack for the steady control case. As α increases, the sensitivity becomes more localized around the upper leading and lower trailing edges of the aerofoil. This would suggest that for a greater angle of attack such as $\alpha = 15°$, the control could be confined to these regions of high sensitivity and requires fewer actuators to practically implement.

Figure 5(b) presents the variation of sensitivities at a fixed angle of attack $\alpha = 10°$ and three of the frequencies identified earlier. For the steady case, there is a smooth distribution with positive sensitivity at the upper leading and lower trailing edges. Around the upper trailing edge, a weak positive sensitivity can be seen however the lower leading edge shows no sensitivity to unsteadiness and therefore could be excluded from the control. The non-zero frequency cases show much greater variance between positive and negative sensitivity, especially around the upper leading edge. This would correspond to a sharp change from blowing to suction over the surface of the aerofoil.

4.3. *Nonlinear control effects of the scaled sensitivity*

From the calculation of the sensitivity (or gradient) of unsteadiness with respect to the control, the linear optimal control to reduce unsteadiness can be obtained from equation (1) by adopting

6

$$u_n = b\boldsymbol{\nabla}_{u_n} A / ||\boldsymbol{\nabla}_{u_n} A||_c$$

where b is a negative scaling factor that reverses and scales the normalized sensitivity as a control. If the value of b, which acts as the control-boundary norm of u_n, is small enough, the control-induced flow is small and can be governed by the linearized NS equation. In this condition, the control induced unsteadiness becomes (Mao and Pearson 2015),

$$\Delta A = \int u_n \boldsymbol{\nabla}_{u_n} A \; d\boldsymbol{C} = b||\boldsymbol{\nabla}_{u_n} A||_c,$$

which is a linear function of the scale factor b. However if $|b|$ exceeds the linear range, the control effects become nonlinear with resect to the magnitude of the control. This nonlinear saturation is verified by varying the value of b and testing the control effects in 2D DNS. Figure 6 presents the results of this study where the change in unsteadiness is plotted as a function of b. Observations show that for $-0.02 \le b \le 0.02$ the change of unsteadiness calculated in 2D DNS agrees well with the linear predictions. However beyond this range, the change in unsteadiness begins to follow a nonlinear pattern until the control approaches a saturated state at $|b| \ge 0.05$.
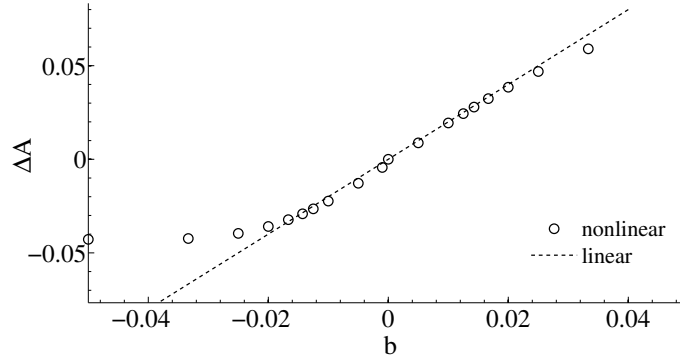
Figure 6.: Change in unsteadiness, denoted as ΔA, due to the linear optimal control with scaling factor b at $\omega = 0$ and $\alpha = 10°$. "linear" denotes the linear predictions $\Delta A = b||\boldsymbol{\nabla}_{u_n} A||_c$ and "nonlinear" represents results extracted from 2D DNS.

The control effects on vortex shedding are shown in figure 7. From figure 7(a) and (b), it is seen that for $b = 0.05$ and $b = 0.02$, where the control is parallel with the sensitivity and tends to increase unsteadiness, the shear layer above the upper surface is forced away from the boundary surface due to the blowing effect and the enlargement of the separation zone results in stronger vortex shedding. Figure 7(c) and (d) represent controlled flow at negative values of b, where the control is in the opposite direction with the sensitivity and tends to reduce unsteadiness. It is seen that at $b = -0.05$, the control completely suppresses the vortex shedding and generates a pair of elongated shear layers downstream of the aerofoil. This result is a product of the applied suction on the fore section of the upper surface (see figure 5), which keeps the shear layers attaching on the body surface and eliminates the recirculation bubble.

4.4. *Control effects to lift and drag*

As shown in figure 6, the control is effective to reduce the unsteadiness and therefore is expected to modify the lift and drag forces to be more steady. The development of controlled and uncontrolled ($b = 0$) forces acting on the aerofoil is shown in figure 8. The controlled forces are calculated as the sum of three parts, i.e. pressure, viscous and thrust forces, where the last one is much smaller
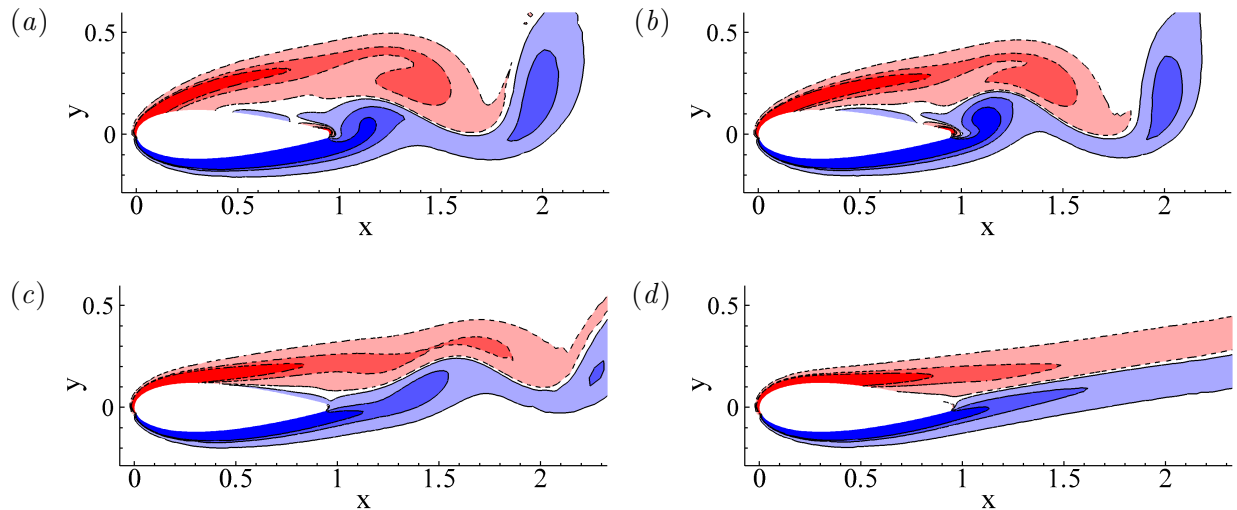
Figure 7.: Contours of controlled spanwise vorticity at $\alpha = 10°$, $\omega = 0$ and scaling factor (a) $b = 0.05$ (b) $b = 0.02$ (c) $b = -0.02$ and (d) -0.05.
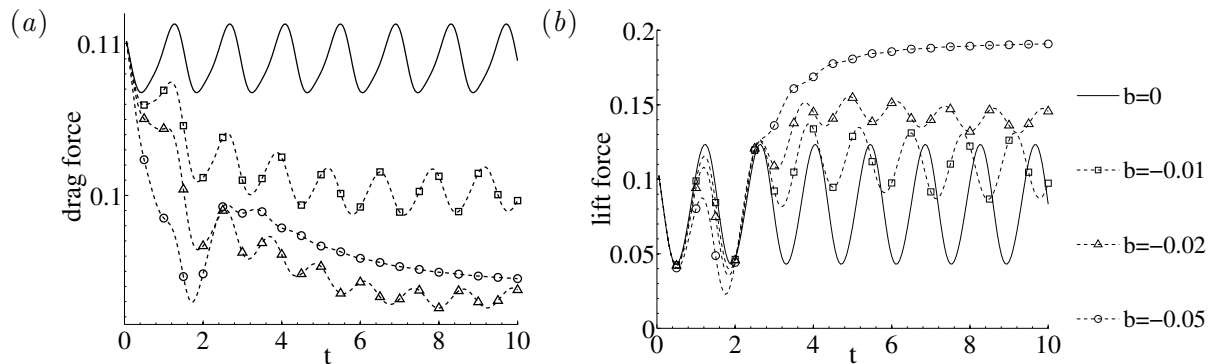
Figure 8.: Optimally controlled (a) drag (b) lift forces at $\omega = 0$ and $\alpha = 10°$.

than the first two and takes less than 2% of the total force over the cases considered. It is clear that the controlled drag/lift force settles to a periodic state with smaller oscillation magnitudes than the uncontrolled ones after an initial transient period. From figure 8(a), it is noticed that as the oscillation of drag is reduced, the mean value also reduces. Comparing against the uncontrolled flow, a drag reduction of 14% is achieved at control scaling factor $b = -0.05$. This improvement in drag can be associated with a decreased pressure on the upper leading edge and an increase in pressure around the trailing edge of the aerofoil. Figure 8(b) presents the relation between the lift force and the increasingly negative control. The increase of mean lift is due to both an increase in pressure on the low surface and a reduction of pressure on the upper surface of the aerofoil. However from this figure, it is clear that the increase in lift due to the control is much greater than the reduction in drag; the lift increases by 138% at a control level of $b = -0.05$. This observation suggests that the lift component of the force is more sensitive to the control than the drag.

The control effects of the linear optimal control obtained at $\alpha = 10^o$ are tested on the out-of-design conditions, as shown in figure 9. It is seen that at $\alpha = 15^o$, the control effect is as clear as in the designed condition $\alpha = 10^o$, in terms of suppression of force fluctuations, drag reduction and lift enhancement. However at $\alpha = 5^o$, the control suppresses the oscillation and increases the mean lift but increases the mean drag slightly. This is because at $\alpha = 5^o$, the vortex shedding and force fluctuations are weak and there is only a tiny recirculation bubble above the upper surface making

8
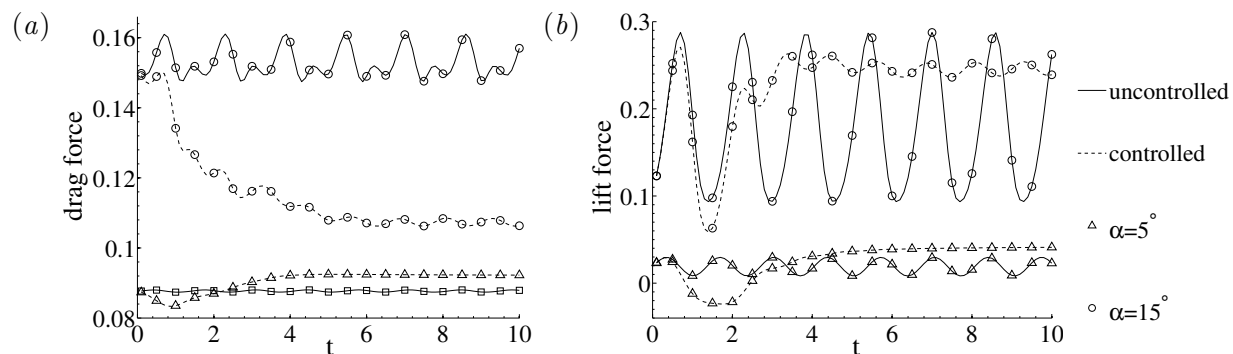
Figure 9.: Controlled (a) drag (b) lift forces at $\omega = 0$ and $b = -0.05$. The control is calculated based on the uncontrolled flow at $\alpha = 10^o$.

the control, in the form of suction around the upper leading edge and targeting at eliminating separation, less effective. This observation suggests that the control calculated at $\alpha = 10^o$ has robust control effects to the operation conditions where boundary layers separate from the surface to form recirculation bubbles, and can be switched off at small angles of attack where the force is almost steady.

5.   Conclusions

The aim of this study is to calculate the linear optimal control that suppresses unsteadiness in flow around a solid body and subsequently oscillations of forces acting on the body via suction and blowing normal to the surface. A modified NACA0024 aerofoil is adopted and the Reynolds number ($Re = 1000$) and angles of attack ($0^o \leq \alpha \leq 15$) considered in this work ensure that the flow is two-dimensional.

The sensitivity of flow unsteadiness with respect to the control is calculated by integrating an adjoint equation, as has been used in explorations of control of hydrodynamic stabilities (Giannetti and Luchini 2007). Then this sensitivity is reversed and scaled to obtain the linear optimal control. By implementing the linear optimal control on the surface of the aerofoil, the control effects on unsteadiness are studied in 2D DNS and the linear range of the magnitude of the control is identified.

It is observed that at scaling factor $b = -0.05$, where the maximum control velocity is less than 8% of the free stream velocity, the separation on the upper surface of the aerofoil and vortex shedding in the domain are completely suppressed at angle of attack $\alpha = 10^o$ and control frequency $\omega = 0$. Extracting forces acting on the aerofoil, it is seen that as the unsteadiness is suppressed, both the lift and drag forces are more steady. As the oscillation of forces is reduced, the mean value of drag (lift) is observed to reduce (increase) simultaneously. At $b = -0.05$, where the unsteadiness is suppressed, a drag reduction of 14% and a lift increase of 138% are observed, suggesting that controlling the unsteadiness significantly improves the aerodynamic performance of the aerofoil.

References

King, R. 1977. "A Review of vortex shedding research and it's application" *Ocean Engng*, 4, 141-171.

Perry, A. E. Chong, M. S. Lim, T. T. 1984. "The vortex-shedding process behind two-dimensional bluff bodies"*J. Fluid Mech*, 116, 77-90.

Bearman, P. W. Graham, J. M. R. 1980. "Vortex shedding from bluff bodies in oscillatory flow: A report on Euromech 119". *J. Fluid Mech*, 9.9, part 2, 226-245.

Ahlborna, B. Setob, M. L. Noackc, B. R. 2002. "On drag, Strouhal number and vortex-street structure". *Fluid Dynamics Research* 30, 379-399.

Bearman, P. W. 1965 "Investigation of the flow behind a two-dimensional model with a blunt trailing edge and fitted with splitter plates". *J. Fluid Mech*, 21, part 2, 241-255.

Kwon, K. Choi, H. 1995. "Control of laminar vortex shedding behind a circular cylinder using splitter plates". *Phys. Fluids 8*, 479-486.

Zdravkovich, M. M. 1981. "Review and classification of various aerodynamic and hydrodynamic means for suppressing vortex shedding". *J. Wind Eng. Ind. Aerodyn*, 7, 145-189.

Chamorro, L. P. Arndt, R.E.A. Sotiropoulos, F. 2013 "Drag reduction of large wind turbine blades through riblets: Evaluation of riblet geometry and application strategies". *Renewable Energy*, 50, 1095-1105.

Mittal, S. Raghuvanshi, A. 2001. "Control of vortex shedding behind circular cylinder for flows at low Reynolds numbers". *Int. J. Numer. Meth. Fluids*, 35, 421-447.

Delaunay, Y. Kaiktsis, L. 2001. "Control of circular cylinder wakes using base mass transpiration". *Phys. Fluids 13*, 3285-3302.

Raju, R. Mittal, R. Cattafesta, L. 2008. "Dynamics of aerofoil separation control using zero-net mass-flux forcing". *AIAA J*, 46, 3103-3115.

Seifert, A. Darabi, A. Wygnanski, I. 1996. "Delay of aerofoil Stall by Periodic Excitation". *Journal of Aircraft*, 33, 691-698.

Modi, V. J. Yokomizo, T. 1994. "On the boundary-layer control through momentum injection: Studies with applications". *Sadhana*,19, part 3, 401-426.

Ongoren, A. Rockwell, D. 1988. "Flow structure from an oscillating cylinder Part 1. Mechanisms of phase shift and recovery in the near wake". *J. Fluid Mech*, 191, 197-223.

Tokumaru, P. T. Dimotakis, P. E. 1991. "Rotary oscillation control of a cylinder wake". *J. Fluid Mech*, 224, 77-90.

Kubo, Y. Modi, V.J. Yasud, H. Kato, K. 1992. "On the suppression of aerodynamic instabilities through the moving surface boundary-layer control". *J. Wind Eng. Ind. Aerodyn*, 41-44, 205-216.

Mao X., Blackburn H. and Sherwin S. 2015. "Nonlinear optimal suppression of vortex shedding from a circular cylinder". *J. Fluid Mech*, in revision.

Mao X. and Pearson E. 2015. "Drag reduction and thrust generation by tangential surface control in flow past a cylinder". *Phys. Fluids*, in revision.

Giannetti, F. Luchini, P. 2007 "Structural sensitivity of the first instability of the cylinder wake". *J. Fluid Mech*, 581, 167-197.

Skote, M. 2013. "Comparison between spatial and temporal wall oscillations in turbulent boundary layer flows". *J. Fluid Mech*, 730, 273-294.

Ricco, P. Hahn, S. 2013. "Turbulent drag reduction through rotating discs". *J. Fluid Mech*, 722, 267-290.